A shared rephasing compass reveals structured local mismatch placement during hyperthermal sarcomeric oscillations

Seine A. Shintani[1,2,3]

[1]Department of Biomedical Sciences, College of Life and Health Sciences, Chubu University, Kasugai, Aichi 487-8501, Japan
[2]Center for Mathematical Science and Artificial Intelligence, Chubu University, Kasugai, Aichi 487-8501, Japan
[3]Institute for Advanced Research, Nagoya University, Nagoya, Aichi 464-8601, Japan

Correspondence: s-shintani@fsc.chubu.ac.jp

Abstract

Neighboring sarcomeres in a cardiomyocyte need not move in perfect synchrony, but it is unclear whether their local timing differences during hyperthermal sarcomeric oscillations (HSOs) are random or organized. Using the same five-sarcomere recordings that previously revealed a constrained 16-state neighboring-pair topology and an amplitude-synchrony relation for the segment-mean rapid signal (Shintani, 2026), we reanalyzed each fast HSO cycle as one local coordination summary. A topology-based circular coordinate showed that the 16 discrete patterns lie on a continuous within-cell order: adjacent positions were enriched for Hamming-1 changes and cycle-to-cycle angular drift was slower than expected by chance. Because each cell has an arbitrary angular zero point and direction, we aligned the cell-wise circles using shared local states as landmarks. This improved same-state concentration across cells from 0.582 to 0.852 ($P = 0.0013$). The clearest biological translation of the aligned coordinate was mismatch placement along the observed five-sarcomere segment. Aligned angle predicted edge-biased mismatch placement (joint $P = 1.15 \times 10^{-6}$), whereas raw angle did not ($P = 0.55$). Beat timing was weaker and signed strain less robust. These findings support a mesoscale view in which local HSO nonuniformity is structured: neighboring sarcomeres share a rephasing order, and that order is most readably expressed by where the local mismatch pocket lies along the chain.

Significance statement

Cardiac contraction must convert noisy local events into a stable beat. This study identifies a measurable intermediate-scale variable in living cardiomyocytes. Fast HSO cycles do not wander randomly among local coordination patterns. After cross-cell alignment, they occupy a shared rephasing compass, and the clearest biological readout of that compass is where a local mismatch pocket sits along the observed five-sarcomere segment. This gives a concrete way to describe how local nonuniformity can remain structured rather than merely disruptive.

Keywords: cardiomyocyte; sarcomere; local coordination; circular coordinate; hyperthermal sarcomeric oscillation

1 Introduction

Cardiac contractility is a multiscale problem. Molecular events are stochastic, yet the cell and the heart still generate an ordered beat. Recent reviews emphasize that this bridge must be understood across scales, from single molecules to whole hearts, and that sarcomeres and myofibrils are key intermediate levels in that chain (Garg et al., 2024; Rassier and Månsson, 2025). The practical question for cell biology is therefore straightforward: how does a cardiomyocyte preserve organized output when its neighboring contractile elements are not perfectly identical?

Direct measurements show that neighboring sarcomeres in living myocardium are heterogeneous in length and strain, that stretch can harmonize part of that heterogeneity, and that sarcomeric synchrony and asynchrony matter for ventricular pump function (Li et al., 2023; Lookin et al., 2023; Kobirumaki-Shimozawa et al., 2021, 2024). These observations also connect to classic length- and strain-dependent activation concepts, in which local mechanics feed back onto myofilament recruitment (de Tombe et al., 2010; Campbell, 2011). Local nonuniformity is therefore not just technical noise. The unresolved issue is whether local timing differences are random or whether they follow a constrained mode of reorganization.

Warmed cardiomyocytes provide a useful setting in which that distinction becomes experimentally visible. Local heat pulses can trigger contraction without detectable calcium transients, microscopic heating can activate cardiac thin filaments directly, and thin-filament activation is strongly cooperative and mechanically regulated (Oyama et al., 2012; Ishii et al., 2019, 2020; Solís and Solaro, 2021; Park-Holohan et al., 2021). HSOs are also related to the broader family of sarcomeric oscillations described under partial activation and SPOC-like conditions (Fabiato and Fabiato, 1978; Linke et al., 1993; Kagemoto et al., 2015). Previous work established that warming induces rapid hyperthermal sarcomeric oscillations (HSOs) while the slower beat-scale rhythm persists (Shintani et al., 2015, 2020; Shintani, 2022, 2025). The HSO state is therefore not just a failure of beating. It is a living-cell regime in which local coordination becomes easier to read.

Our recent reanalysis of the same five-sarcomere recordings provided two anchors for that regime (Shintani, 2026). First, local rearrangements occupied a constrained 16-state neighboring-pair topology dominated by Hamming-1 transitions, meaning that only one neighboring relation usually changed at a time. Second, the segment-mean rapid signal was closely described by the product of local oscillation size and weighted synchrony, $A \times R_w$. Those results showed that local irregularity is structured and that segment-level output depends on how local motion is coordinated. What they did not explain was why cycles sharing the same coarse local state could still differ in behavior.

That remaining variation suggested that the 16 labels might sit on an additional continuous order. To test that idea, we used a persistent-homology-based circular coordinate. In plain terms, this method asks whether the cloud of cycle-wise local states forms a loop-like arrangement and, if so, where each cycle sits on that loop (de Silva et al., 2011). Because each cell can place the zero point and direction of that circle arbitrarily, we then aligned the circles across cells using shared local states as landmarks.

The message of this follow-up is intended to be simple. Local HSO nonuniformity is better described as a shared rephasing order than as random fluctuation or a disconnected list of binary patterns. The clearest physiological reading of that order is where the local mismatch pocket is positioned along the observed five-sarcomere segment.

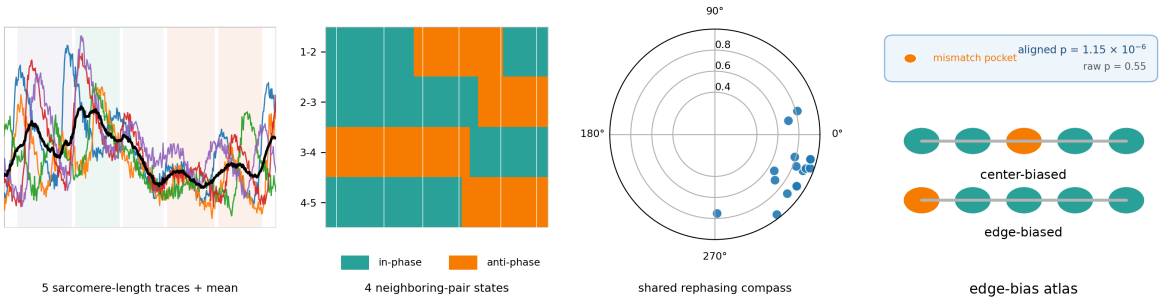

Graphical abstract. Five consecutive sarcomere-length traces were condensed into one local coordination summary per fast HSO cycle. A topology-based circular coordinate revealed a within-cell order, and cross-cell alignment turned that order into a shared rephasing compass. The clearest biological translation of that compass was where the local mismatch pocket was positioned along the observed five-sarcomere segment.

2 Results

2.1 Each fast HSO cycle is converted into one local coordination summary

Figure 1 first makes the analytical unit explicit. Five consecutive sarcomere-length traces from one exemplar HSO window were centered around the cell-specific HSO band, converted to instantaneous phase, and reduced to four neighboring-pair relations. Within the phase-valid gate, each neighboring pair was classified as in-phase or anti-phase. Each fast HSO cycle was then summarized as one row in a cycle-wise table. That row stores a dominant four-link local pattern together with its circular position, aligned circular position, pooled aligned sector, beat-phase position, and mismatch-placement summaries. This step matters because all later analyses remain anchored to directly observed fast cycles rather than to a hidden-state model.

Three terms are used repeatedly below. First, the **signal-survival ratio** asks how much of the local rapid amplitude survives averaging into the segment-mean rapid signal; at cycle level it is Y_{valid}/A. Second, **Stopo** is a coarse synchrony score derived from the same four-link binary pattern under an equal-amplitude $0/\pi$ assignment. It takes values of 1.0, 0.6, or 0.2, with smaller values meaning stronger cancellation in the segment mean if amplitudes were equal. Third, **aligned sectors 1–4** are four equal quarter-circle bins of the aligned circular coordinate used only for pooled summaries. They are summary bins, not additional biological states.

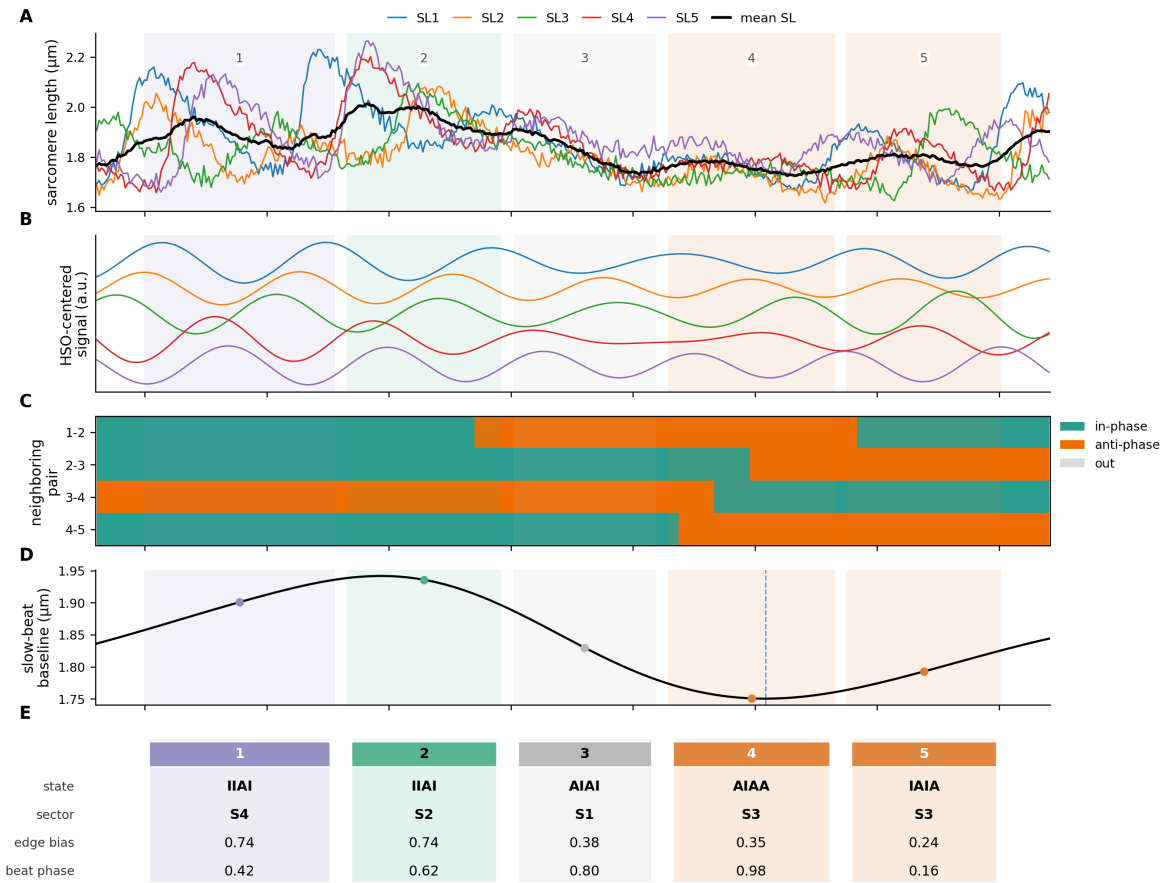

Figure 1: Each fast HSO cycle is converted into one local coordination summary. Representative sarcomere-length traces from one cell are converted into the analysis unit used throughout the manuscript. The figure shows the raw five-sarcomere traces and their mean, the HSO-centered internal signals, the four neighboring-pair in-phase/anti-phase assignments, the slow-beat baseline used to locate each fast cycle, and the final one-cycle-one-row table. Each row stores a dominant local state, a raw circular coordinate, an aligned circular coordinate, a pooled aligned sector, beat-phase position, and mismatch-placement summaries. The numbered example rows are display labels for this figure only.

2.2 Discrete local patterns also lie on a continuous within-cell loop

We next asked whether the 16 neighboring-pair patterns are merely a catalog of discrete labels or whether they also occupy an ordered continuum (Figure 2). To connect the local patterns to the observed rapid signal, we summarized each dominant state by its **state-mean signal-survival ratio**, namely the mean fraction of local rapid amplitude that survives averaging into the segment mean for cycles assigned to that state. States with the same Stopo still showed substantial differences in this quantity, indicating that the coarse synchrony class alone does not exhaust the biology.

The circular-coordinate analysis revealed a clear within-cell order beneath the 16-state description. Adjacent positions on the recovered circle were enriched for Hamming-1 changes (0.504 vs 0.284 under a null ordering, paired $P = 0.0156$). Within a given fast cycle, occupied local states clustered within a narrow angular sector (within-cycle circular concentration 0.985 vs 0.702 under shuffle, paired $P = 0.0078$), and cycle-to-cycle movement along the circle was slow rather

than random (mean $|\Delta\theta| = 0.285$ rad vs 0.844 rad under shuffle, paired $P = 0.0078$). Adding circular-angle terms to Stopo improved per-cell explanation of state-mean signal-survival ratio (mean R^2 0.158 $\rightarrow$ 0.443), and adding simple boundary-geometry terms improved it further (0.158 $\rightarrow$ 0.538).

The biological interpretation is therefore mixed but readable. Local HSO dynamics do use a finite set of neighboring-pair patterns, but those patterns also lie on a continuous rephasing loop. Figure 2B and Figure 3B answer complementary questions. Figure 2B asks whether one cell contains such a loop at all. Figure 3B asks whether different cells share the same loop order after alignment.

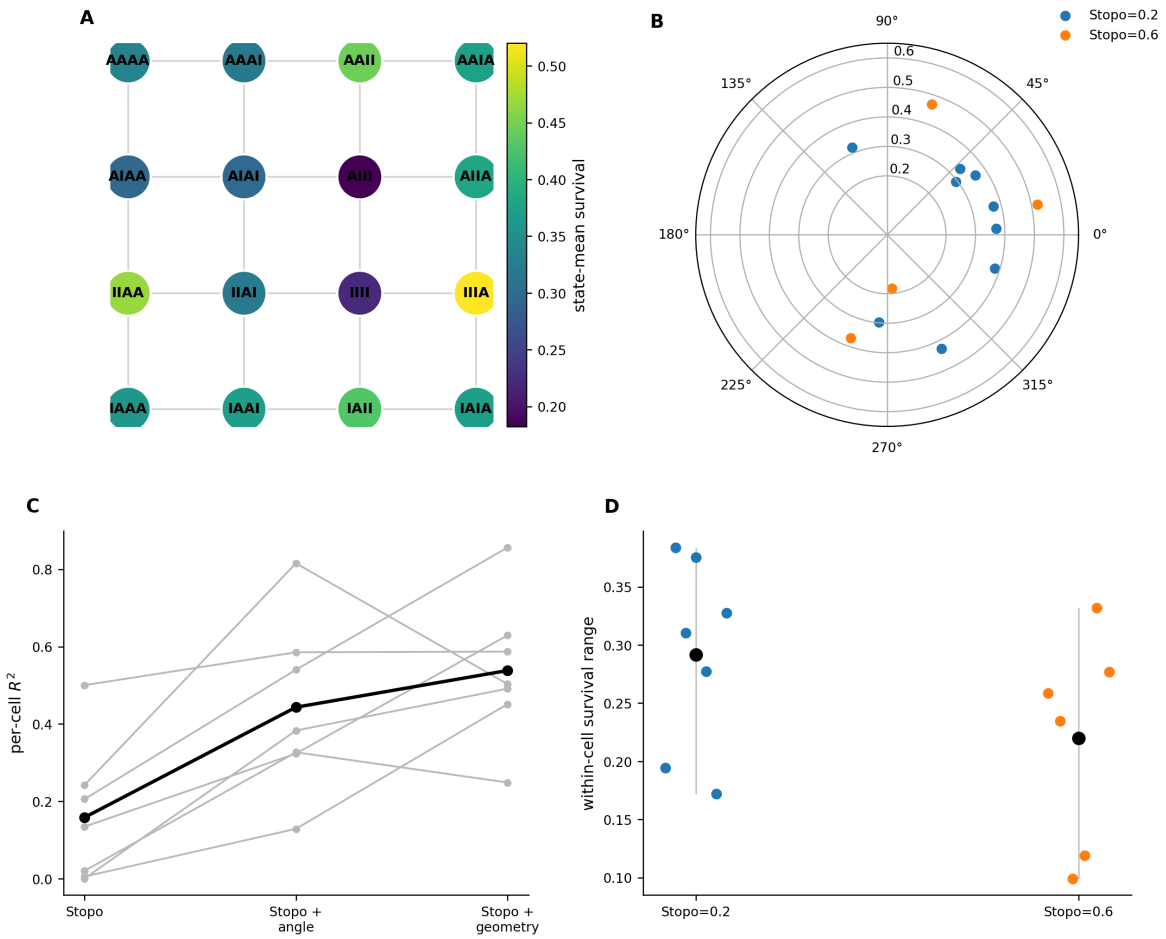

Figure 2: Discrete local patterns also lie on a continuous within-cell loop. (A) Hamming-1 network of the 16 neighboring-pair patterns. Each label lists the four neighboring pairs from 1–2 to 4–5, with I = in-phase and A = anti-phase. Node color shows the state-mean signal-survival ratio, defined as the mean fraction of local rapid amplitude that survives into the segment-mean rapid signal for cycles dominated by that state. (B) Within one exemplar cell, each occupied local state is placed on the raw circular coordinate recovered from persistent homology. Angle therefore shows where that state sits on the within-cell loop. Radius shows the state-mean signal-survival ratio from panel A. Point color shows Stopo, a coarse state-derived synchrony score computed from the same binary pattern under an equal-amplitude $0/\pi$ phase assignment. Stopo = 1.0 means complete reinforcement of the segment mean, whereas Stopo = 0.6 and 0.2 indicate progressively stronger cancellation. (C) Per-cell R^2 for models of state-mean signal-survival ratio using Stopo alone, Stopo plus circular-angle terms, and Stopo plus simple boundary-geometry terms. (D) Within-cell range of state-mean signal-survival ratio among states that share the same Stopo, showing that states within the same coarse synchrony class are not functionally equivalent.

2.3 Cross-cell alignment reveals a shared rephasing compass

The raw circular coordinate is informative within one cell, but its zero point and direction are arbitrary and therefore cannot be pooled directly across cells. We therefore aligned the cell-wise circles using shared local states as landmarks (Figure 3). After alignment, same-state concentration—the degree to which the same labeled state occupies one common angle across cells—improved from 0.582 to 0.852 (paired $P = 0.0013$), and the median same-state angular deviation narrowed from 0.696 rad to 0.271 rad. Rotation alone improved concentration partway (0.810), but full alignment performed best.

The functional gain was likewise visible only after alignment. In models of state-centered signal-survival ratio, adding raw sector did not improve the fit ($P = 0.334$), whereas adding aligned sector did ($P = 0.017$). In models of state-centered Y_{valid}, raw sector again failed to help ($P = 0.292$), whereas aligned sector did ($P = 0.002$). In other words, the pooled structure is not already present in the raw cell-wise angles; it emerges when the circles are put onto a common compass.

We therefore use the term **shared rephasing compass**. The aligned coordinate should not be read as an absolute physiological angle with its own independent meaning. Rather, it is a common ordering of local mismatch configurations that becomes comparable across cells.

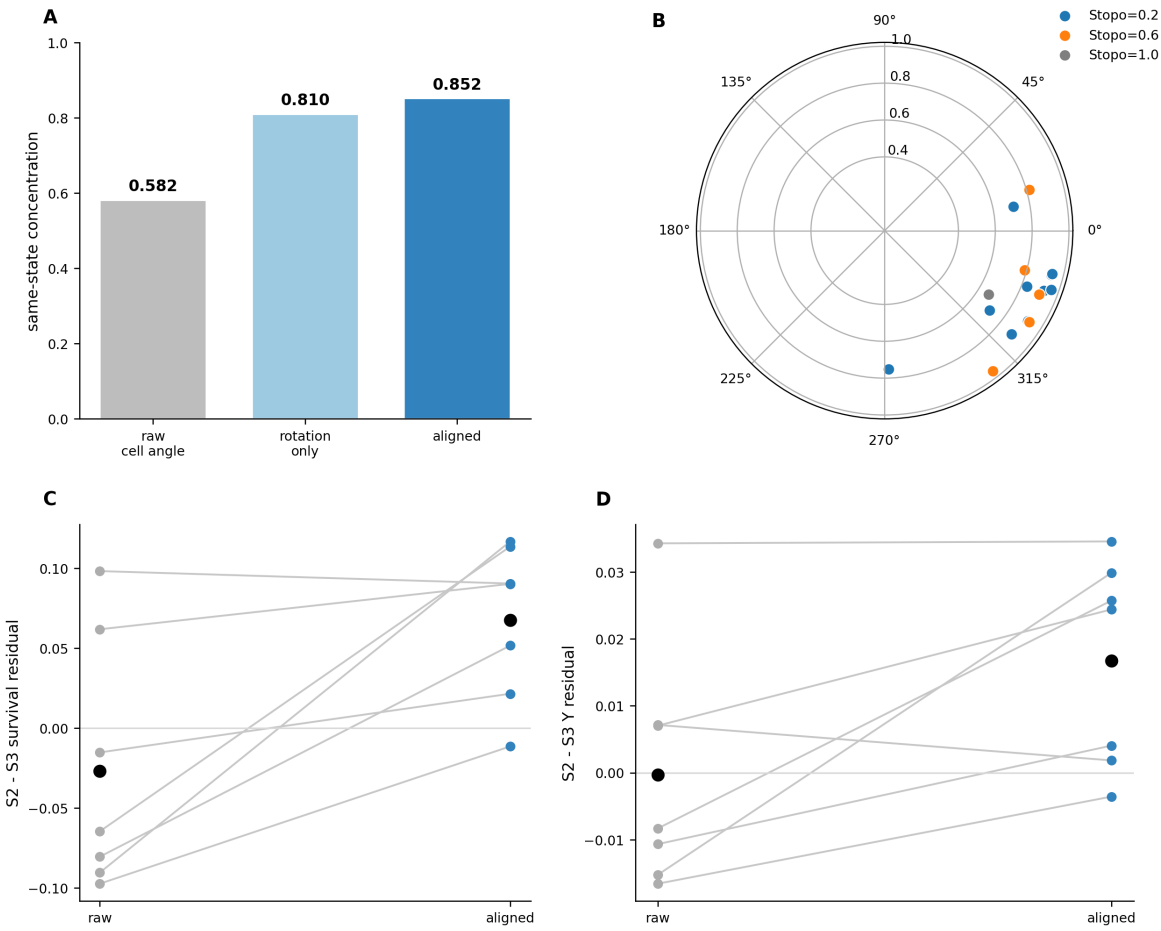

Figure 3: Cross-cell alignment reveals a shared rephasing compass. (A) Same-state concentration across cells before and after alignment. (B) Shared-state atlas after alignment. Each point is one occupied local state pooled across cells after alignment. Angle shows the aligned atlas position of that state, and radius shows same-state concentration across cells. Point color again shows Stopo. This panel answers a different question from Figure 2B: Figure 2B asks whether one cell contains a loop-like order, whereas Figure 3B asks whether different cells share the same order after alignment. (C) Paired cell-wise difference in residual signal-survival ratio between aligned sectors 2 and 3, shown before and after alignment. (D) Paired cell-wise difference in residual segment-mean rapid amplitude (Y_{valid}) between aligned sectors 2 and 3, shown before and after alignment. For pooled summaries, aligned sectors 1–4 are four equal quarter-circle bins of the aligned circular coordinate. They are summary bins, not additional biological states.

2.4 The shared compass is translated most strongly into mismatch placement

We then asked what this shared compass means in ordinary physiological language (Figure 4). Within one fast cycle, if one phase class forms a minority cluster, we call that cluster the **mismatch pocket**. We summarize its position with a mismatch-placement bias score, where positive values indicate that the minority-phase pocket is positioned closer to one end of the observed five-sarcomere segment than to its center. Here, **edge** refers to an end of the observed five-sarcomere segment, not to the cell boundary.

Among the candidate translations we tested, mismatch placement along the chain was the strongest. Aligned angle strongly predicted edge-biased mismatch placement (joint $P = 1.15 \times 10^{-6}$), whereas the raw-angle control was null ($P = 0.55$). Beat timing also varied across

the shared compass, but more weakly (aligned $P = 0.0124$; raw $P = 0.727$). Signed end-to-end strain asymmetry pointed in the same broad direction but was weaker and more fragile (aligned $P = 0.0425$; raw $P = 0.472$). When the aligned circle was summarized into four pooled sectors, the clearest contrast appeared between sectors 2 and 3. These sectors differed in signal-survival ratio, Y_{valid}, mismatch placement, and beat timing, whereas the corresponding raw-sector summaries remained null.

The most accessible reading is therefore not simply that cycles differ by an abstract angle. The shared compass most clearly tells us where the local out-of-step pocket tends to sit within the chain.

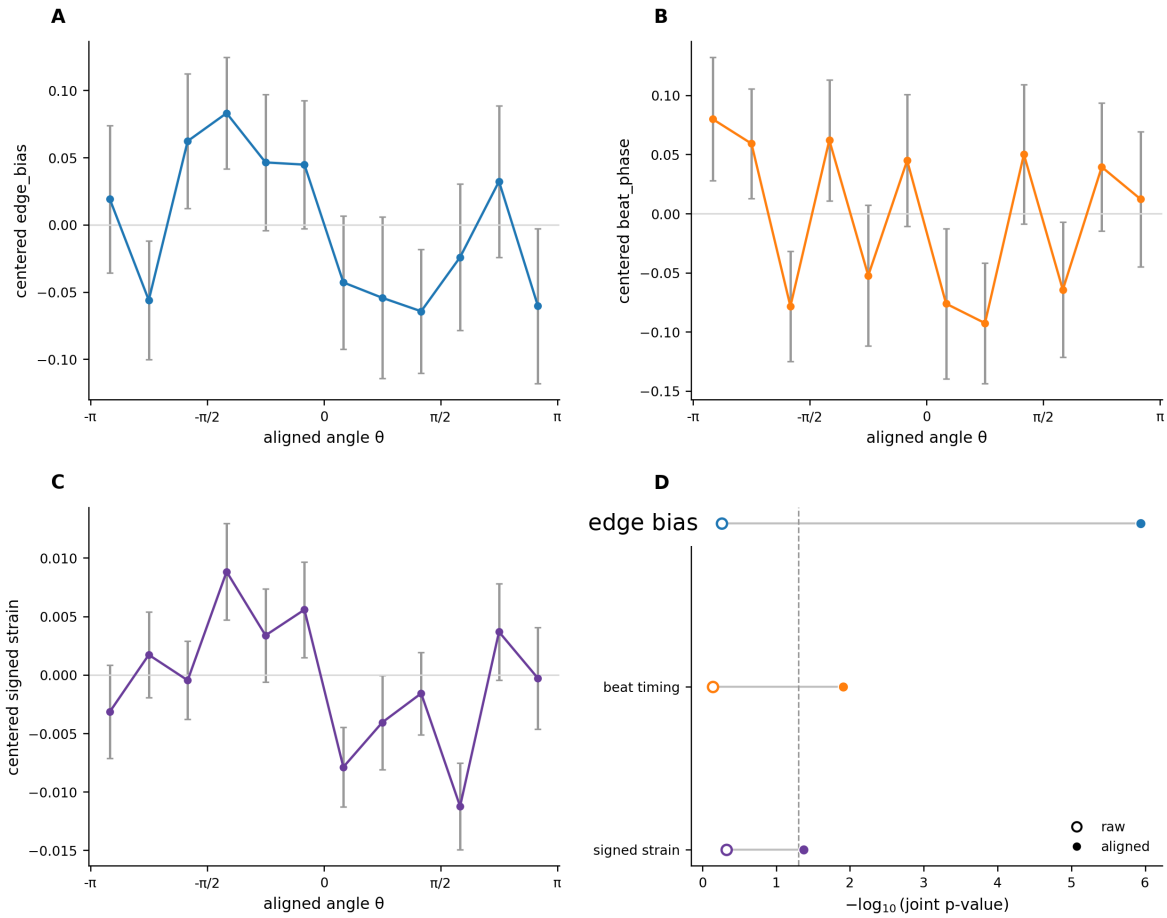

Figure 4: The shared compass is translated most strongly into mismatch placement. (A–C) Means and standard errors of centered mismatch-placement bias, centered beat-phase position, and centered signed end-to-end strain asymmetry across bins of the aligned circular coordinate. Positive mismatch-placement bias means that the minority-phase cluster is positioned closer to one end of the observed chain than to its center. Here, edge refers to an end of the observed five-sarcomere segment, not to the cell boundary. (D) Raw-versus-aligned joint P-value comparison for the three translation variables. Mismatch placement is the strongest and most robust translation of the shared rephasing compass. Beat timing is weaker, and signed strain is the weakest of the three.

2.5 Robustness analyses rank the claims and limit over-interpretation

Sensitivity analyses were used to rank the claims rather than to inflate them (Figure 5). A prespecified influential-cell sensitivity analysis was carried out because the earlier cycle-level

work had identified one quality-control issue in one sarcomere trace. In that analysis, edge-biased mismatch placement remained the strongest result, whereas beat timing weakened to borderline significance and signed strain weakened further. The stricter same-exact-state mismatch-placement law also weakened in the same sensitivity analysis. Mirror-assignment tests showed that signed strain depended strongly on left–right assignment, whereas edge-biased mismatch placement did not.

This ranking is important for how the manuscript should be read. The main biological claim is the shared rephasing compass together with mismatch placement along the observed chain. Beat timing is a secondary translation of the same compass. Signed strain and the stricter exact-state law are informative, but they are best treated as supportive rather than central.

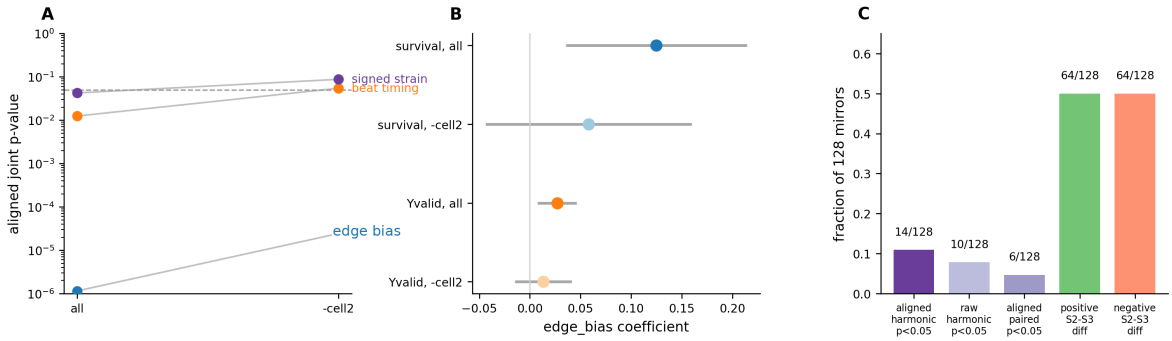

Figure 5: Robustness analyses rank the claims. (A) Harmonic angle effects for mismatch placement, beat timing, and signed strain in the full dataset and in the influential-cell sensitivity analysis. (B) Exact-state mismatch-placement coefficients for signal-survival ratio and Y_{valid} in the full dataset and in the influential-cell sensitivity analysis. (C) Mirror-assignment sensitivity for signed strain. These analyses justify treating mismatch placement as the main-text claim, beat timing as a secondary translation, and signed strain plus the exact-state law as supportive rather than central.

3 Discussion

The central result of this study is that local HSO nonuniformity is not best described as random noise. Neighboring sarcomeres do not simply wander among unrelated local patterns. Instead, the observed five-sarcomere segment occupies a shared rephasing compass, and the clearest physical reading of that compass is where the local mismatch pocket is positioned along the chain. In plain biological language, the segment appears to redistribute local mismatch rather than merely tolerate it.

This matters because cardiac contractility is a middle-scale problem. Molecular events are stochastic, whereas beat-scale output is comparatively stable. Reviews of cardiac contractility and myosin mechanics emphasize the need to connect single molecules, sarcomeres, myofibrils, cells, and whole hearts within one mechanistic framework (Garg et al., 2024; Rassier and Månsson, 2025). This interpretation is also consistent with the chaordic homeodynamics framework proposed for sarcomere-level periodic chaos, in which stable beat-scale behavior coexists with structured microscopic variability (Shintani, 2025). The present work does not solve that entire multiscale bridge, but it identifies a measurable mesoscale variable within it.

In this dataset, the most robust mesoscale readout is mismatch placement along the observed chain.

The result is also coherent across several analytical levels. The same recordings first show minimal one-pair switching, then a loop-like within-cell order, then improved same-state concentration after cross-cell alignment, and finally a clear ranking of biological translations with mismatch placement at the top. That sequence argues against the idea that the atlas is merely a small-sample statistical skew. The conclusion does not rest on one isolated association. It rests on several independent analyses that point in the same direction.

The physiological message is not that sarcomeres are either perfectly synchronized or hopelessly disordered. Instead, the data support a softer and more useful picture in which local mismatch is redistributed in a rule-governed way. This interpretation fits with the broader view that local sarcomere heterogeneity is biologically meaningful rather than incidental, and it suggests one concrete way in which a beating cell may preserve organized segment-level behavior while still allowing local flexibility (Li et al., 2023; Kobirumaki-Shimozawa et al., 2021, 2024).

The hierarchy of claims should remain explicit. The strongest result is mismatch placement along the observed chain. Beat timing aligns with the same shared compass but is less robust. Signed strain and the stricter same-exact-state law are biologically interesting, but they do not yet support the same level of confidence. Making that ranking visible is part of what keeps the manuscript readable and trustworthy.

Several limitations define the appropriate level of interpretation. The study analyzes seven cells and one observed five-sarcomere line segment per cell. The present analysis does not establish a whole-cell propagation law, and the aligned compass should be read as a quantitative working description rather than as a final general law. Longer line segments, independent datasets, and simultaneous measurements of local Ca^{2+}, force, and titin-related mechanics will be needed to test how general this mesoscale organization is and how it is produced.

4 Conclusion

Fast HSO cycles in living cardiomyocytes are not adequately described as random transitions among disconnected local states. They occupy a shared rephasing compass that becomes comparable across cells after alignment. The clearest biological translation of that compass is where the local mismatch pocket is positioned along the observed five-sarcomere segment. This gives a concrete mesoscale variable for thinking about how local sarcomere heterogeneity can remain structured while segment-level output is preserved.

5 Materials and methods

5.1 Study design, data source, and ethics

This study is a follow-up reanalysis of previously acquired sarcomere-length data from neonatal rat cardiomyocytes. No new animal experiments were performed for the present work. The original experimental procedures were approved by the Animal Experiment Committee of the Faculty of Science at the University of Tokyo and were conducted according to the Animal Experiment Implementation Manual of the University of Tokyo, as reported previously (Shintani et al., 2020; Shintani, 2026). The reanalyzed dataset consisted of seven cells, with one observed five-sarcomere line segment analyzed in each cell.

5.2 Original cell preparation and microscopic system

The original experimental procedures have been described in detail elsewhere (Shintani et al., 2014, 2015, 2020). Briefly, immature cardiomyocytes were isolated from 1-day-old Wistar rats and cultured in DMEM/F-12 containing 10% fetal bovine serum, penicillin, and streptomycin. Cells expressed α-actinin-AcGFP, and measurements were performed one day after transfection. Imaging used an inverted microscope equipped with a high-sensitivity camera and an oil-immersion objective. The pixel size in the specimen plane was 150 nm, and the frame rate was 500 frames/s. A 1550-nm laser was used as a local heat source, and a 488-nm laser was used to excite AcGFP-actinin fluorescence.

5.3 Signal decomposition and local-state definition

For each cell, the HSO fundamental frequency was estimated from the HSO segment by spectral analysis of the root-mean-square internal signal. Each sarcomere trace was centered by subtracting the instantaneous local mean of the five observed sarcomeres and then band-pass filtered around the cell-specific HSO-centered band. Instantaneous phase and amplitude envelope were obtained from the Hilbert transform. Phase-valid intervals were defined from the mean high-frequency envelope using a hysteresis gate.

At each phase-valid time point, the five-sarcomere segment was represented by the four neighboring-pair phase relations 1–2, 2–3, 3–4, and 4–5. A neighboring pair was classified as in-phase when $\cos(\Delta\phi) \geq 0$ and anti-phase when $\cos(\Delta\phi) < 0$. The four binary neighboring-pair relations yielded 16 possible local phase patterns. Fast HSO cycles were then summarized as one row per cycle, storing the dominant local state together with beat-phase position, circular coordinate, aligned sector, mismatch-placement bias, and local mechanical summaries.

5.4 Signal-survival ratio, Stopo, and cycle-wise averaged measurements

To connect local patterns to the segment-mean rapid signal, we defined the cycle-level **signal-survival ratio** as the fraction of local rapid amplitude that survives averaging into the observed

segment mean. In variable names, this quantity was Y_{valid}/A, where A is the mean peak-to-peak HSO amplitude across the observed sarcomeres within a cycle and Y_{valid} is the peak-to-peak HSO amplitude of the observed-segment mean trace in the same cycle.

Stopo was used as a coarse synchrony score derived directly from the binary local pattern. For each 16-state pattern, we assigned the five sarcomeres to two phase groups under an equal-amplitude $0/\pi$ assignment implied by the four neighboring-pair relations and computed the magnitude of the resulting normalized segment mean. This yielded Stopo = 1.0, 0.6, or 0.2, with lower values meaning stronger cancellation under the equal-amplitude assumption.

5.5 Circular coordinate, cross-cell alignment, and pooled sectors

Within each cell, persistent-homology / circular-coordinate analysis was used to derive a loop-like local rephasing coordinate from the cycle-wise state cloud (de Silva et al., 2011). Because the raw circular coordinate has arbitrary origin and direction, cell-wise coordinates were aligned across cells using shared occupied local states as landmarks. For pooled summary plots only, the aligned circular coordinate was divided into four equal bins, denoted aligned sectors 1–4. These sectors are summary bins and were not treated as additional biological states.

5.6 Translation variables and statistics

Mismatch-placement bias quantified how close the minority-phase pocket was to one end of the observed chain relative to its center. Beat-phase position located the same cycle on the slow-beat baseline. Signed end-to-end strain asymmetry summarized the difference between the two ends of the observed segment but was interpreted cautiously because it depends on left–right assignment.

Pooled linear models used cell fixed effects. Circular predictors were encoded with cosine and sine terms, and joint tests were used for angle effects. Cell-wise paired summaries used Wilcoxon signed-rank tests. A prespecified influential-cell sensitivity analysis repeated the key models after excluding cell 2 because the earlier cycle-level analysis had identified one sarcomere trace in that cell as a mean-length outlier. Additional robustness checks included exact-state models and mirror-assignment sensitivity analyses for signed strain.

Author contributions

S.A.S. conceived the study, performed the original experiments and the present reanalysis, and wrote the manuscript.

Funding

This work was supported by JSPS KAKENHI Grant Number JP25K00269 (Grant-in-Aid for Scientific Research (C), project title: "Elucidation of Myosin Molecular Dynamics Associated with Sarcomere Morphological Changes in the Intracellular Environment").

Declaration of interests

The author declares no competing interests.

Data and code availability

The reanalyzed dataset, the figure-level summary tables used for the present analyses, and the custom analysis code used in this study are available from the corresponding author upon reasonable request.

Declaration of generative AI and AI-assisted technologies in the writing process

During the preparation of this work, the author used ChatGPT (OpenAI) to improve the readability and language of the manuscript. After using this tool, the author reviewed and edited the content as needed and takes full responsibility for the content of the publication.

References

Shintani, S.A. 2026. Constrained neighboring-sarcomere phase topology shapes mean HSO amplitude in living cardiomyocytes. *bioRxiv*. doi: 10.64898/2026.03.13.711515.

Garg, A., K.J. Lavine, and M.J. Greenberg. 2024. Assessing cardiac contractility from single molecules to whole hearts. *JACC Basic Transl. Sci.* 9:414–439. doi: 10.1016/j.jacbts.2023.07.013.

Rassier, D.E., and A. Månsson. 2025. Mechanisms of myosin II force generation: insights from novel experimental techniques and approaches. *Physiol. Rev.* 105:1–93. doi: 10.1152/physrev.00014.2023.

Li, J., J. Sundnes, Y. Hou, M. Laasmaa, M. Ruud, A. Unger, T.R. Kolstad, M. Frisk, P.A. Norseng, L. Yang, I.E. Setterberg, E.S. Alves, M. Kalakoutis, O.M. Sejersted, J.T. Lanner, W.A. Linke, I.G. Lunde, P.P. de Tombe, and W.E. Louch. 2023. Stretch harmonizes sarcomere strain across the cardiomyocyte. *Circ. Res.* 133:255–270. doi: 10.1161/CIRCRESAHA.123.322588.

Lookin, O., P. de Tombe, N. Boulali, C. Gergely, T. Cloitre, and O. Cazorla. 2023. Cardiomyocyte sarcomere length variability: membrane fluorescence versus second harmonic generation myosin imaging. *J. Gen. Physiol.* 155:e202213289. doi: 10.1085/jgp.202213289.

Kobirumaki-Shimozawa, F., T. Shimozawa, K. Oyama, S. Baba, J. Li, T. Nakanishi, T. Terui, W.E. Louch, Shin'ichi Ishiwata, and N. Fukuda. 2021. Synchrony of sarcomeric movement regulates left ventricular pump function in the in vivo beating mouse heart. *J. Gen. Physiol.* 153:e202012860. doi: 10.1085/jgp.202012860.

Kobirumaki-Shimozawa, F., K. Oyama, T. Nakanishi, Shin'ichi Ishiwata, and N. Fukuda. 2024. Asynchronous movement of sarcomeres in myocardium under living conditions: role of titin. *Front. Physiol.* 15:1426545. doi: 10.3389/fphys.2024.1426545.

Fabiato, A., and F. Fabiato. 1978. Myofilament-generated tension oscillations during partial calcium activation and activation dependence of the sarcomere length–tension relation of skinned cardiac cells. *J. Gen. Physiol.* 72:667–699. doi: 10.1085/jgp.72.5.667.

Linke, W.A., M.L. Bartoo, and G.H. Pollack. 1993. Spontaneous sarcomeric oscillations at intermediate activation levels in single isolated cardiac myofibrils. *Circ. Res.* 73:724–734. doi: 10.1161/01.RES.73.4.724.

Kagemoto, T., A. Li, C. dos Remedios, and S. Ishiwata. 2015. Spontaneous oscillatory contraction (SPOC) in cardiomyocytes. *Biophys. Rev.* 7:15–24. doi: 10.1007/s12551-015-0165-7.

Oyama, K., A. Mizuno, S.A. Shintani, H. Itoh, T. Serizawa, N. Fukuda, M. Suzuki, and Shin'ichi Ishiwata. 2012. Microscopic heat pulses induce contraction of cardiomyocytes without calcium transients. *Biochem. Biophys. Res. Commun.* 417:607–612. doi: 10.1016/j.bbrc.2011.12.015.

Ishii, S., K. Oyama, T. Arai, H. Itoh, S.A. Shintani, M. Suzuki, F. Kobirumaki-Shimozawa, T. Terui, N. Fukuda, and Shin'ichi Ishiwata. 2019. Microscopic heat pulses activate cardiac thin filaments. *J. Gen. Physiol.* 151:860–869. doi: 10.1085/jgp.201812243.

Ishii, S., K. Oyama, S.A. Shintani, F. Kobirumaki-Shimozawa, Shin'ichi Ishiwata, and N. Fukuda. 2020. Thermal activation of thin filaments in striated muscle. *Front. Physiol.* 11:278. doi: 10.3389/fphys.2020.00278.

Solís, C., and R.J. Solaro. 2021. Novel insights into sarcomere regulatory systems control of cardiac thin filament activation. *J. Gen. Physiol.* 153:e202012777. doi: 10.1085/jgp.202012777.

Park-Holohan, S.-J., E. Brunello, T. Kampourakis, M. Rees, M. Irving, and L. Fusi. 2021. Stress-dependent activation of myosin in the heart requires thin filament activation and thick filament mechanosensing. *Proc. Natl. Acad. Sci. USA* 118:e2023706118. doi: 10.1073/pnas.2023706118.

de Tombe, P.P., R.D. Mateja, K. Tachampa, Y.A. Mou, G.P. Farman, and T.C. Irving. 2010. Myofilament length dependent activation. *J. Mol. Cell. Cardiol.* 48:851–858. doi: 10.1016/j.yjmcc.2009.12.017.

Campbell, K.S. 2011. Impact of myocyte strain on cardiac myofilament activation. *Pflügers Arch. Eur. J. Physiol.* 462:3–14. doi: 10.1007/s00424-011-0952-3.

de Silva, V., D. Morozov, and M. Vejdemo-Johansson. 2011. Persistent cohomology and circular coordinates. *Discrete Comput. Geom.* 45:737–759. doi: 10.1007/s00454-011-9344-x.

Shintani, S.A., K. Oyama, F. Kobirumaki-Shimozawa, T. Ohki, Shin'ichi Ishiwata, and N. Fukuda. 2014. Sarcomere length nanometry in rat neonatal cardiomyocytes expressed with α-actinin-AcGFP in Z discs. *J. Gen. Physiol.* 143:513–524. doi: 10.1085/jgp.201311118.

Shintani, S.A., K. Oyama, N. Fukuda, and Shin'ichi Ishiwata. 2015. High-frequency sarcomeric auto-oscillations induced by heating in living neonatal cardiomyocytes of the rat. *Biochem. Biophys. Res. Commun.* 457:165–170. doi: 10.1016/j.bbrc.2014.12.077.

Shintani, S.A., T. Washio, and H. Higuchi. 2020. Mechanism of contraction rhythm homeostasis for hyperthermal sarcomeric oscillations of neonatal cardiomyocytes. *Sci. Rep.* 10:20468. doi: 10.1038/s41598-020-77443-x.

Shintani, S.A. 2022. Hyperthermal sarcomeric oscillations generated in warmed cardiomyocytes control amplitudes with chaotic properties while keeping cycles constant. *Biochem. Biophys. Res. Commun.* 611:8–13. doi: 10.1016/j.bbrc.2022.04.055.

Shintani, S.A. 2025. Chaordic homeodynamics: the periodic chaos phenomenon observed at the sarcomere level and its physiological significance. *Biochem. Biophys. Res. Commun.* 760:151712. doi: 10.1016/j.bbrc.2025.151712.